Renewable Energy 153 (2020) 1378–1395

Contents lists available at ScienceDirect

Renewable Energy

journal homepage: www.elsevier.com/locate/renene

Revision of hydrothermal constraints for the installation of closed-loop shallow geothermal systems through underground investigation, monitoring and modeling

Rodolfo Perego [a, b, *], Diego Viesi [c], Sebastian Pera [a], Giorgia Dalla Santa [b], Matteo Cultrera [b], Paola Visintainer [d], Antonio Galgaro [b]

[a] Institute of Earth Sciences, University of Applied Sciences and Arts of Southern Switzerland (SUPSI), Campus Trevano, CH-6952, Canobbio, Switzerland
[b] Department of Geosciences, Università degli Studi di Padova, Via Gradenigo 6, 35131, Padova, Italy
[c] Applied Research on Energy Systems (ARES), Fondazione Bruno Kessler (FBK), Via Sommarive 18, I-38123, Povo, Trento, Italy
[d] Geological Survey, Autonomous Province of Trento, Via Zambra 42, 38122, Trento, Italy

ARTICLE INFO

Article history:
Received 27 September 2019
Received in revised form
5 February 2020
Accepted 18 February 2020
Available online 21 February 2020

Keywords:
Hydrothermal constraints
Shallow geothermal energy
Ground source heat pump
3D geothermal modeling
Underground thermal interference

ABSTRACT

The hydrothermal area of Ponte Arche (Italian Alps) hosts favorable geothermal conditions and presence of thermal water, which is used for therapeutic purposes. Political constraints are in force, since the district is classified as "potentially subject to geothermal manifestations". The Government of the Province of Trento exceptionally approved a pilot shallow geothermal closed-loop system: underground investigations and high spatial-temporal resolution monitoring were performed in order to assess the absence of thermal interference between the installed borefield and the neighboring hydrothermal wells. Acquired thermo-geological and energetic information were conveyed into a numerical model devoted to predict the long-term thermal behavior of the system, detecting the potential arise of thermal interference towards hydrothermal wells. Before the long-term analysis (50 years), the numerical model was doubly validated against both short-term and medium-term response. The simulation of the long-term real-case scenario shows that the thermal plume developed by the system is limited to a diameter of 74 m, while for a long-term heating-only scenario it is limited to a maximum diameter of 96 m. Long-term results for both real and heating-only scenario show that under no circumstances the experimental closed-loop system would interfere with the neighboring hydrothermal wells distant 610, 1350 and 1450 m.

1. Introduction

Geothermal energy is one of the main renewable energy sources in terms of ubiquity and energetic potential: several technologies can use this energy source to produce electricity and/or heat depending on the working temperatures and depending on the presence or absence of local geothermal anomalies. While the electricity generation usually requires temperatures above 150 °C, available only in some favorable geological settings, the heat generation is an option available everywhere thanks to the coupling with ground source heat pumps (GSHP). Moreover, a GSHP system is able to both extract heat from the underground and inject heat into the underground, the latter applicable for cooling. Two categories of GSHPs are generally recognized: open-loop systems, through the exploitation of groundwater pumped by dedicated wells, and closed-loop systems, that use ground heat exchangers (GHEs) installed in the subsurface. The most common solution for closed loop systems is adopting vertical borehole heat exchangers (BHEs) [1].

These systems can produce a thermal impact on the subsurface temperature, since they act as a heat sink in winter or a heat source in summer. Depending on their size and their energy demand, they can produce a small or large thermal impact. Moreover, BHEs can also produce environmental impacts by connecting different aquifers if not properly backfilled, swelling of particular geological formations [2] or subsidence. Due to these potential issues their installation or maximum depth is in some cases restricted [3],

* Corresponding author. Institute of Earth Sciences, University of Applied Sciences and Arts of Southern Switzerland (SUPSI), Campus Trevano, CH-6952, Canobbio, Switzerland.
E-mail address: rodolfo.perego@supsi.ch (R. Perego).

https://doi.org/10.1016/j.renene.2020.02.068
0960-1481/

Abbreviations and symbols

BHE	Borehole Heat Exchanger
CEIS	Consorzio Elettrico Industriale Stenico
DHW	Domestic Hot Water
DSO	Distribution System Operator
GHE	Ground Heat Exchanger
GSHP	Ground Source Heat Pump
MAE	Mean Absolute Error
NZEB	Nearly Zero Energy Building
PED	Primary Energy Demand
PV	Photovoltaic
R_a	External thermal resistance (mK/W)
R_b	Borehole thermal resistance (mK/W)
RMSE	Root Mean Squared Error
SC	Space Cooling
SH	Space Heating
Ss	Specific storage (1/m)
T_g	Ground temperature (°C)
TRT	Thermal Response Test
VHC	Volumetric Heat Capacity (MJ/m^{3}K)
VSP	Vertical Seismic Profile
ΔT	Temperature variation (°C)
λ	Thermal conductivity (W/mK)
ϕ	Porosity

especially in groundwater protection areas to preserve groundwater quality for drinking or leisure purposes [4,5].

Intuitively, local temperature variations produced by BHE operation strongly depend on size/energy demand and local geological/hydrogeological conditions. These perturbations are called thermal plumes and can be divided into cold and hot plumes, depending on the different running season with, respectively, heat extraction or injection [6]. Different methods are used to evaluate the induced underground thermal plume, such as geophysical or direct measures on monitoring wells. The extent, shape and magnitude of these thermal plumes can be analytically estimated only for small systems and for simplified scenarios, while numerical modeling becomes necessary when evaluating large systems with complex geological/hydrogeological conditions and high temporal/spatial resolutions.

The analyzed case study is situated in an area surrounding the village of Ponte Arche, located in the Province of Trento, Italy. The particular geological setting allows the groundwater to transport heat from the depths to the surface, achieving a significant hydrothermal circulation and, hence, creating a thermal bath area with several hotels dedicated to health and wellness. The sustainable use of the natural hydrothermal source must be protected by carefully assessing the potential coexistence with other types of subsoil exploitation, including open and closed-loop geothermal systems. Theoretically these shallow geothermal systems could produce thermal plumes and therefore interfere with the already installed hydrothermal wells. This could happen if they are too close to the protected catchments, if their operation substantially affects the thermal status of the subsurface, specially through markedly imbalanced energy demand (utilization of the stored heat without a proper restoration or heat injection without proper drawing) or if particular hydrogeological conditions contribute to propagate the thermal plume far away from the geothermal system. To this purpose, the area of Ponte Arche is currently subject to the absolute prohibition for BHEs installation according to the regulation currently in force in the Province of Trento. However, the local interest in closed-loop systems has strongly increased in recent years. In particular, in 2013 the local electrical Distribution System Operator (DSO), Consorzio Elettrico Industriale Stenico (CEIS), became directly interested in disseminating the BHE technology as an attractive solution to provide building conditioning and domestic hot water (DHW), both in summer and winter, in a sustainable way: a “green” alternative to the use of fossil fuels. Therefore, CEIS proposed to the local geological survey the overcoming of the strict regulatory constraints by installing a new experimental monitored BHE field at its headquarters, located within the area of Ponte Arche. This paper supports the CEIS experimental study coupling a spatial/temporal high-resolution geothermal monitoring with a numerical modeling approach.

3D numerical modeling related to closed-loop shallow geothermal systems has been extensively used in the past years for a large number of applications worldwide. Fujii et al. (2007) [7] developed regional scale and local scale numerical models to produce GSHP suitability maps for the Chikushi plain (Japan); Hein et al. (2016) [8] built a representative model of Leipzig city (Germany) to understand the impact of GSHP design errors; Tang and Nowamooz (2018) [9] studied the long-term performance of a GSHP system located in Alsace (France), a region with favorable geothermal conditions; Daemi and Krol (2019) [10] assessed the thermal plumes for a GSHP system in Canada, observing different extents for different operating conditions; Dalla Santa et al. (2019) [11] showed the importance of considering freeze-thaw effects for BHE modeling in case of low working temperature (Italy); Epting et al. (2013) [12] built a regional model to assess the thermal influences of geothermal systems on the urban aquifer of Basel city (Switzerland). Cultrera et al. (2017) [13] used numerical modeling in the framework of a preliminary methodology to define the main parameters of shallow aquifers by using heat as tracer. Galgaro et al., in 2015 [14] investigated the sustainability of a hypothetical BHE array within the Euganean thermal Basin (Italy). The numerical model simulated the potential thermal interference of the BHE field on the neighboring hydrothermal wells exploited by spa and resorts, stating that the thermal plume reaches some extraction wells but without causing significant alteration of the temperature of the extracted water. However, in that case no experimental data were shown to validate the numerical model outputs: the present paper also focuses on improving this aspect.

Among these applications, it is very rare to find studies that focus on the use of shallow geothermal numerical modeling to tackle political or resource management issues. Usually numerical or GIS modeling are applied in the context of spatial management of shallow subsurface resources only when delineating the extension of wellheads protection zones, as described in Refs. [15–18]. The present work focuses on studying the opposite phenomenon: given the well-established hydrothermal constraints in form of protection zones, this study wants to make the most of shallow geothermal monitoring and geological/hydrogeological modeling in order to assess potential spatial interactions of the installed closed-loop vertical system on the protected catchments. More in detail, the aim is to determine that the heat exchange processes caused by the BHE array do not significantly impact the thermal baths. Depending on the results of the monitoring data and on the long-term modeling outputs, the administration could consider the revision of the current protection criteria and the hydrothermal constraints map, thus evaluating the authorization of other BHEs in the area.

In this work the finite elements modeling is implemented by means of the numerical code FEFLOW [19] that allows hydrodynamic and thermodynamic analysis, including the simulation of conductive and convective heat transport inside porous media under both saturated and unsaturated conditions. Compared to the monitoring analysis, the numerical modeling analysis provides two important advantages in terms of space and time. It provides the evolution of the thermal alteration spatially induced in the underground in a 3D volume of appropriate size, thus evaluating the impact in a wide area and not only in some limited vertical monitoring wells. In addition, it estimates the induced thermal alteration in the long-term, then projecting short-term monitoring results over time. On the other hand, the measured monitoring data acquired on site are fundamental to calibrate and validate the modeling analysis in short term scenarios, thus obtaining a robust and reliable model, to be applied for forecast the behavior in the long-term.

The present work represents a novelty in the shallow geothermal energy research since it couples multi-year high-resolution monitoring and validated numerical modeling, with the aim of demonstrating the sustainability of closed-loop shallow geothermal systems and to improve spatial management of the subsurface even in constrained areas.

2. The hydrothermal area of Ponte Arche

In the following paragraphs, the main features of the case study are described: the geological setting and the test building (CEIS headquarters). Further information about these two aspects is extensively described in Viesi et al., 2018 [20].

2.1. Geological setting

From the geological standpoint, in the investigated area (Fig. 1) few meters of superficial Quaternary fluvio-glacial deposits (mixed materials from silt/clay to sand/gravel, of fluvial or glacial origin) are followed by marly clays called “Argille di Ponte Arche” (with a thickness that can be up to 500 m [21]). Moreover, being the CEIS headquarters placed close to a fault line on which the river Duina is set, the rocks are frequently fractured due to tectonic stresses. The study area is placed at the core of a syncline, it is also the most depressed area occupied by rocks with low permeability, while the carbonate sides are characterized by high permeability. The regional hydrogeological setting is therefore quite simple: the percolation water, guided by the disjunctive grating and by the main structural features that intersect the carbonate masses placed at NW and SE of the waterproof core, penetrates deep and feed the carboniferous aquifer, which sustains the package of marls and marly clays. Therefore, the local stratigraphy and tectonic guarantees isolation for the groundwater of the carboniferous aquifer. The natural manifestation of the hydrothermalism is represented by the spring called Antica Fonte. The spring is located on the eastern side of the syncline, where the waterproof covering shows the minimum thickness, it has a bicarbonate-calcic chemistry, the average flow rate is 3 l/s and the temperature is 27 °C [22].

2.2. The test building: CEIS headquarters

From 2013 to 2015, the electrical DSO of Ponte Arche, called CEIS, refurbished its headquarters with a Nearly Zero Energy Building (NZEB) vision. The new building has a volume of 2038 m^3 and a net floor area of 516 m^2 (Fig. 2). As part of the renovation works, an electric GSHP has been integrated with 5 double-U BHEs. The BHEs have a depth of 125 m each and are positioned about 10 m away from each other (S1 to S5 in Fig. 2), in order to avoid mutual thermal interference [23]. Moreover, an additional 150 m BHE named S6, not operational, was placed near the operative BHE field (17 m away from S1), in order to monitor the underground temperature. The multifunctional GSHP, absorbing and releasing heat through the BHEs, allows both to heat (18.5 kW) and to cool (26.7 kW) the entire building, also including the DHW (Domestic Hot Water) production. Moreover, 2 PV systems of 12 kW each are dedicated respectively to the electric demand of the GSHP and to other CEIS electrical devices. Approximately 30% of the GSHP

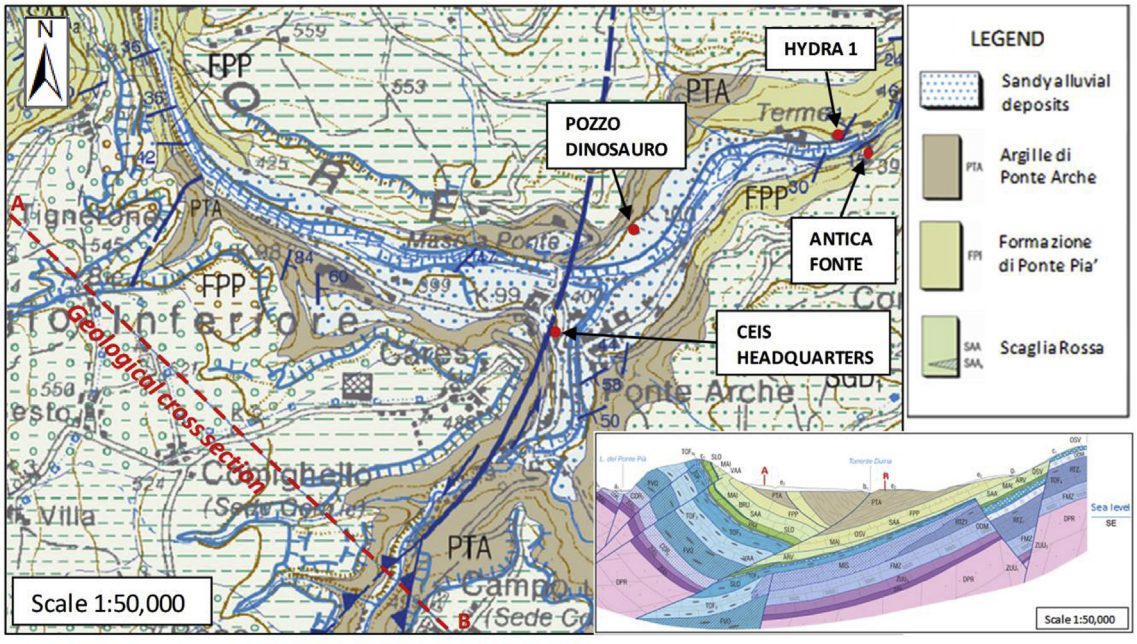

Fig. 1. Geological sheet “CARG 059 Tione di Trento” with the case study and hydrothermal wells locations. For more information on the geological setting of the area the reader is referred to Ref. [20] (image modified after [20]).

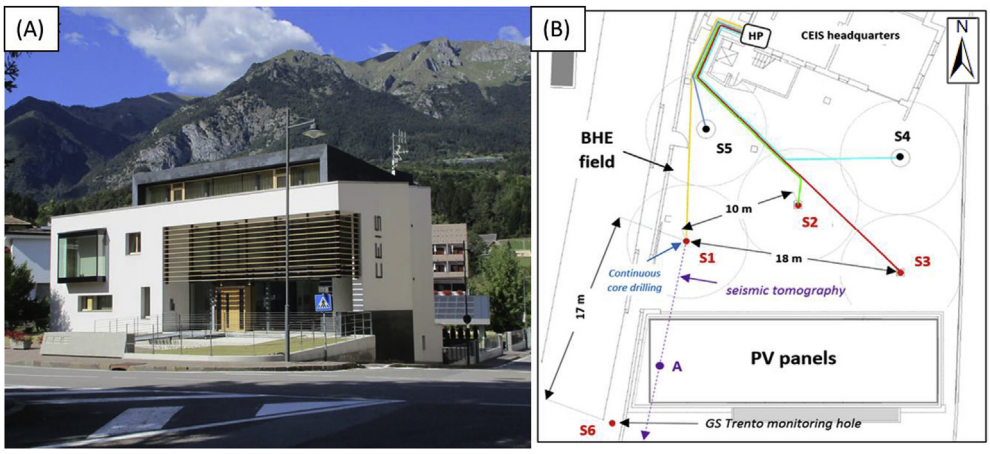

Fig. 2. (A) The CEIS headquarters. (B) Layout of the GSHP system.

electricity demand is planned to be satisfied by using the PV system. The thermal design of the building identifies as prevalent the space heating (SH) demand, with an annual value of 19.6 MWh, the space cooling (SC) is slightly lower with 12.2 MWh/year, whilst the DHW is very low (1.5 MWh/year) considering the office use of the building. The thermal sustainability performance of the new NZEB CEIS headquarters is significantly improved in comparison with the old CEIS headquarters (for the complete characteristics of the old CEIS headquarters, the reader is referred to Ref. [20]): annual Primary Energy Demand (PED) 3.68 kWh/m^3 vs 21.23 kWh/m^3, annual CO_2 emissions 0.15 t vs 9.29 t, annual energy cost 692 € vs 3429 €.

The CEIS headquarters is located in an area potentially affected by hydrothermal manifestations (Fig. 3 [24]), for the current legislation this implies a ban for the drilling of BHEs. However, by resolution n. 2134 October 11th of 2013, the Government of the Province of Trento authorized the installation of the CEIS BHE field as a local experimental study in order to evaluate the underground thermal interference, especially towards Comano thermal baths [25]. New geological and hydrogeological knowledge (underground investigation), monitoring data and modeling analysis are under evaluation for the potential review of the protection criteria and of the extent of the area where BHE installation is prohibited.

3. Methods

The methodological approach applied in this work is divided into three phases: underground investigation, experimental geothermal monitoring and numerical modeling.

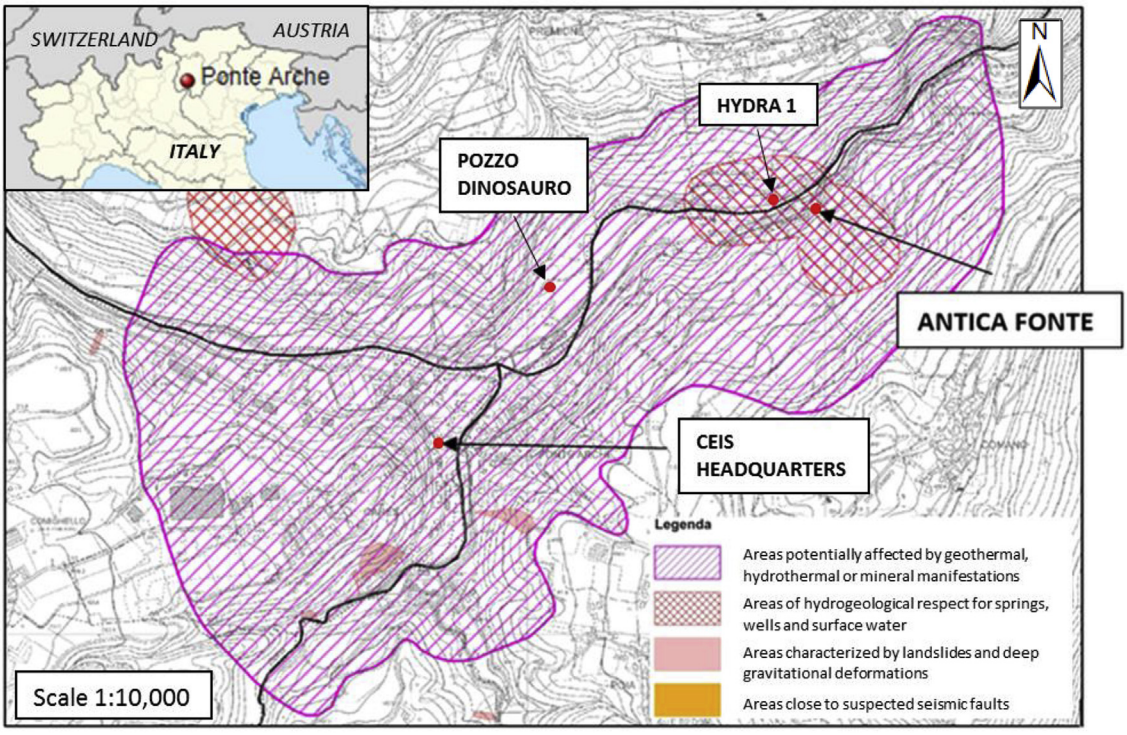

Fig. 3. Regional view of the position of the investigated study area compared with the nearby hydrothermal wells. The purple hatch represents the "area potentially affected by hydrothermal manifestations". The red areas represent the "hydrogeological respect area for springs, wells and surface waters". Image modified after [20]. Source: [24].

3.1. Underground investigation

To deepen the knowledge of the local geological setting, at the beginning of the experimental study some on-site surveys were performed:

- drilling with continuous core (depth 125 m);
- three downhole geophysical surveys (vertical seismic profile, T log, electric conductivity log);
- thermal response test (TRT).

The continuous core drilling (Fig. 4), which corresponds to the BHE S1, confirms the local stratigraphy. On the surface, a few meters of fluvio-glacial deposits show a wide grain size distribution, sands and gravels are alternated with silts and clays. Within the fluvio-glacial deposits the groundwater level is approximately 3 m b.g.l. Proceeding downwards, the bedrock depth is detected at 10.10 m. From 10.10 m down to the hole bottom (at the depth of 125 m from the surface) only one rock formation is identified, the "*Argille di Ponte Arche*", composed by marly clays: some of these layers show high fracturation.

In S1 downhole geophysical surveys were performed: they include one temperature log, one electric conductivity log and one vertical seismic profile (VSP) (Fig. 4) [26]. Slumping of the inner walls of S1 stopped the temperature and the electric conductivity logs at 98 m while the VSP at 72 m.

The temperature and the electric conductivity logs were realized in S1, water filled from a depth of 4.8 m. The obtained results show that the seasonal thermal perturbation affects the first 16 m. Below there is a slight negative temperature gradient down to the depth of 50 m, where the measured temperature reaches the minimum of 10.6 °C. From here, a positive gradient of 0.68 °C/100m up to 75 m is shown. At this depth, the temperature increases associated with a reduction of the electric conductivity can be potentially ascribed to the incoming of groundwater from fractured rocks. Finally, the geothermal gradient in the range 75–98 m shows a slight increase in comparison with the previous range, with a value of 1.1 °C/100m. The VSP was performed with a chain of 24 hydrophones, spaced 1m, introduced into the S1. Four surface energizations where applied, extending the VSP analysis down to a depth of 72m. Fig. 4 (C) detects the presence of a superficial aerated soil for 8–10 m (low seismic speeds), above the rock (high seismic speeds). Correlating the continuous core drilling with the VSP, the intervals with high fracturation display the lower seismic speeds. Furthermore, the intervals with high fracturation appear to be laterally discontinuous, thus the characteristics found in S1 could be different in the other wells.

Based on the S1 stratigraphy and considering relevant bibliography ([27,28]), the thermophysical properties in S1 are reported in Table 1. Moreover, thermophysical characteristic and BHEs performance were explored by means of a TRT [29] performed on the BHE S2 (see Fig. 1). In the first phase of the test the underground undisturbed temperature (T_g) was measured to be 13.5 °C. For the identification of λ (thermal conductivity) and R_b (borehole thermal resistance) the duration of the TRT was 70 h, applying a heat input of 5593 W. The identified values were: $\lambda = 2.69$ W/mK, $R_b = 0.10$ mK/W. The TRT λ is about 30% higher than the bibliographic λ. The reasons may be the following: different bibliographic vs real lithologies or a convective contribution by the groundwater moving through fractured layers ([30–32]).

3.2. Experimental geothermal monitoring

The monitoring layout includes the CEIS building (BHE temperatures, GSHP ground-side heat flow, outdoor climatic temperature) and 3 hydrothermal wells (called Pozzo Dinosauro, Hydra1 and Antica Fonte, distant respectively 610, 1350 and 1450 m from the CEIS building, monitoring of groundwater temperatures), in

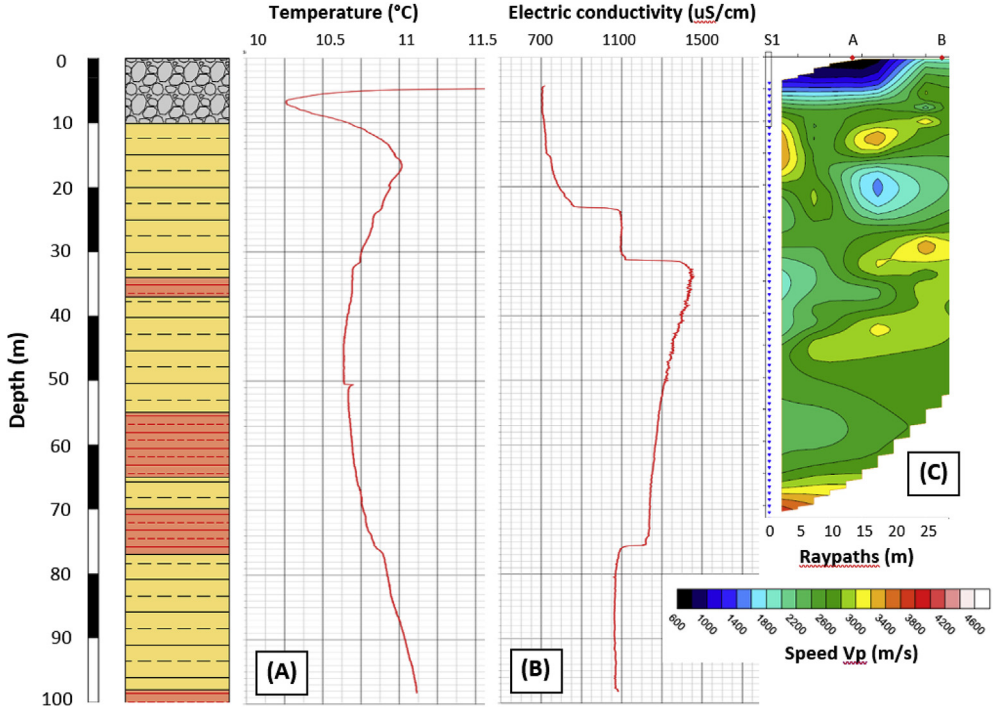

Fig. 4. Comparison of the S1 continuous core drilling stratigraphy with the downhole geophysical surveys: temperature (A), electric conductivity (B), seismic tomography (C). Data from GG Service, [26]. Fluvio-glacial cover is represented in grey, while argillites characterized by low and high fracturation are reported respectively in yellow and orange. Iimage modified after [20]. (For interpretation of the references to colour in this figure legend, the reader is referred to the Web version of this article.)

Table 1
Comparison between the thermal properties of the subsurface estimated by bibliography and measured from the TRT. ([27,28,33]).

Lithology	Depth (m)	Bibliography	In-situ temperature	Thermal Response Test	Bibliography	Thermal Response Test	Bibliography
		T (°C)	T (°C)	T (°C)	λ (W/mK)	λ(W/mK)	Volumetric Heat Capacity (MJ/m^3K)
Unconsolidated deposits (unsaturated)	0–3				0.4		1.48
Unconsolidated deposits (saturated)	3–10.10				2.10		2.28
Argillites	10.10 –125				2.10		2.25
Weighted average (only for thermal properties)	**0–125**	**11.51**	**10.87**	**13.5**	**2.06**	**2.69**	**2.23**

order to detect the BHE thermal influence on the hydrothermal area (see Fig. 3).

More in detail, the monitoring system of the CEIS building consists in: (I) the monitoring of the underground temperature in 3 active BHEs (S1, S2 and S3, as represented in Fig. 1), (II) the monitoring of the underground temperature in the non-active BHE S6, (III) the monitoring of the GSHP ground-side heat flow, (IV) the monitoring of the outdoor climatic temperature. In the underground monitoring, Pt100 sensors are located close to the external polyethylene surface of the BHEs every 20 m of depth and for greater safety and accuracy two sensors are provided at each measurement depth.

The CEIS monitoring system is active since March 4th, 2014, firstly (4/3/2014–31/8/2014) in a reduced layout (S1 operative, S2 and S3 only monitoring), starting from April 2nd, 2015 in the full version. With a time-frequency of 10 min, all the measured values are collected through a NI CompactRIO data logger that at the end of each day produce and store a daily csv file, saved both in a local and in a remote memory. The Pt100 sensors have an accuracy of ±0.06 °C at 0 °C (class 1/5B) while the 4 wires acquisition with the NI 9217 modules guarantees typical accuracy of ±0.15 °C. Therefore, the overall accuracy of the underground monitoring is ±0.21 °C; thermal fluctuations within this range cannot be ascribed specifically to any natural or anthropogenic reason.

3.3. Proposed methodology

The proposed methodology to assess potential interference of a new pilot closed-loop geothermal system on current hydrothermal spatial constraints is reported in Fig. 5. The method starts with the creation of a monitoring system in the hydrothermal wells that must be protected from thermal alteration. The suggested workflow foresees the creation of a short-term and medium-term numerical model. After the reliability assessment of both the short-term and medium-term models, long-term scenarios could be simulated. If none of the simulated scenarios show thermal impacts on the protected hydrothermal wells, a revision of the spatial constraints could be proposed. Vice versa if thermal impact is simulated only in the worst-case scenario, the legislator can decide whether or not to approve the revision of the geothermal constraints depending on the precautionary principle [34].

3.4. Numerical modeling

First, a simulation of the TRT executed on February 5th, 2014 at probe S2 was performed, comparing measured and simulated outlet temperatures in order to understand the reliability of the proposed model response in simulating short-term phenomena. Subsequently, a three years simulation from 2ndof April 2015 to 31st of March 2018 was performed by using daily aggregations of real monitored data of thermal powers and flow rates ground-side. Some sensitivity analysis was performed in order to understand what are the major parameters affecting the extent of the thermal plume. In probe S6 (see Fig. 1) the results of the simulation were validated against real monitored underground temperature, to understand the reliability of the proposed three years model. Finally, a 50 years long-term analysis of thermal impact produced by the BHE array was executed, by simulating both the real case scenario with balanced heating/cooling building requests and a heating-only scenario, assuming the absence of underground thermal restoration through a cooling period. The choice of this simulation timeframe, which is longer than a suggested period of 30 years [1], was selected in order to dissipate all the doubts regarding a potential thermal unsustainability of the geothermal system. Moreover, the heating-only scenario was performed to simulate a critical situation in order to test the long-term feasibility of the system even for a strongly unbalanced thermal load.

3.4.1. Spatial discretization

The 3D groundwater flow and heat transport model was built using the numerical code FEFLOW, version 7.2 [19]. The horizontal domain is a square of 120 m side (adequate for a BHE field with a maximum width of 20 m), the total investigated area is therefore 14,400 m^2. The square size was set according to the most probable groundwater system, even without taking into account the nearby Duina river whose hydraulic and hydrogeological boundary conditions were little known. The 120*120 m mesh was refined in the center, on the BHE array area, in order to obtain a more accurate evaluation of the temperature changes due to the heat exchangers influence [35]. When using numerical solutions for both long-term simulations (quasi-stationary model of Eskilson & Claesson [36]) and short-term ones (Al-Khoury [37]), the BHE is reduced to a boundary condition limited to a single mesh node. This assumption leads to some modeling consequences: the creation of a series of standardized mesh points around the boreholes allows having the virtual radius equal to the physical radius and a more accurate solution: this particular optimization of the mesh around BHE is particularly important when simulating short-term processes such as TRTs. For a borehole diameter of 0.152 m, as in this case, node distance is equal to 0.47 m. The mesh check was performed by ensuring that no Delaunay criterion violations were observed, an appropriate mean of maximum interior angle of triangles (73.2°) was reached and a low mean condition number (5.61) was achieved. The final refinement of the BHEs is highlighted in Fig. 6a.

A Digital Elevation Model (DEM) with a horizontal spatial resolution of 20 m, provided by the Province of Trento, was used to assign elevation values to the upper slice of the domain. The vertical discretization was performed according to the geothermal conceptual model with a vertical refinement set at the lithological transition between fluvio-glacial deposits and the sedimentary rock and at the BHE bottom (125m depth). A total of 53 slices and therefore 52 layers parallel to the surface were created from the bi-

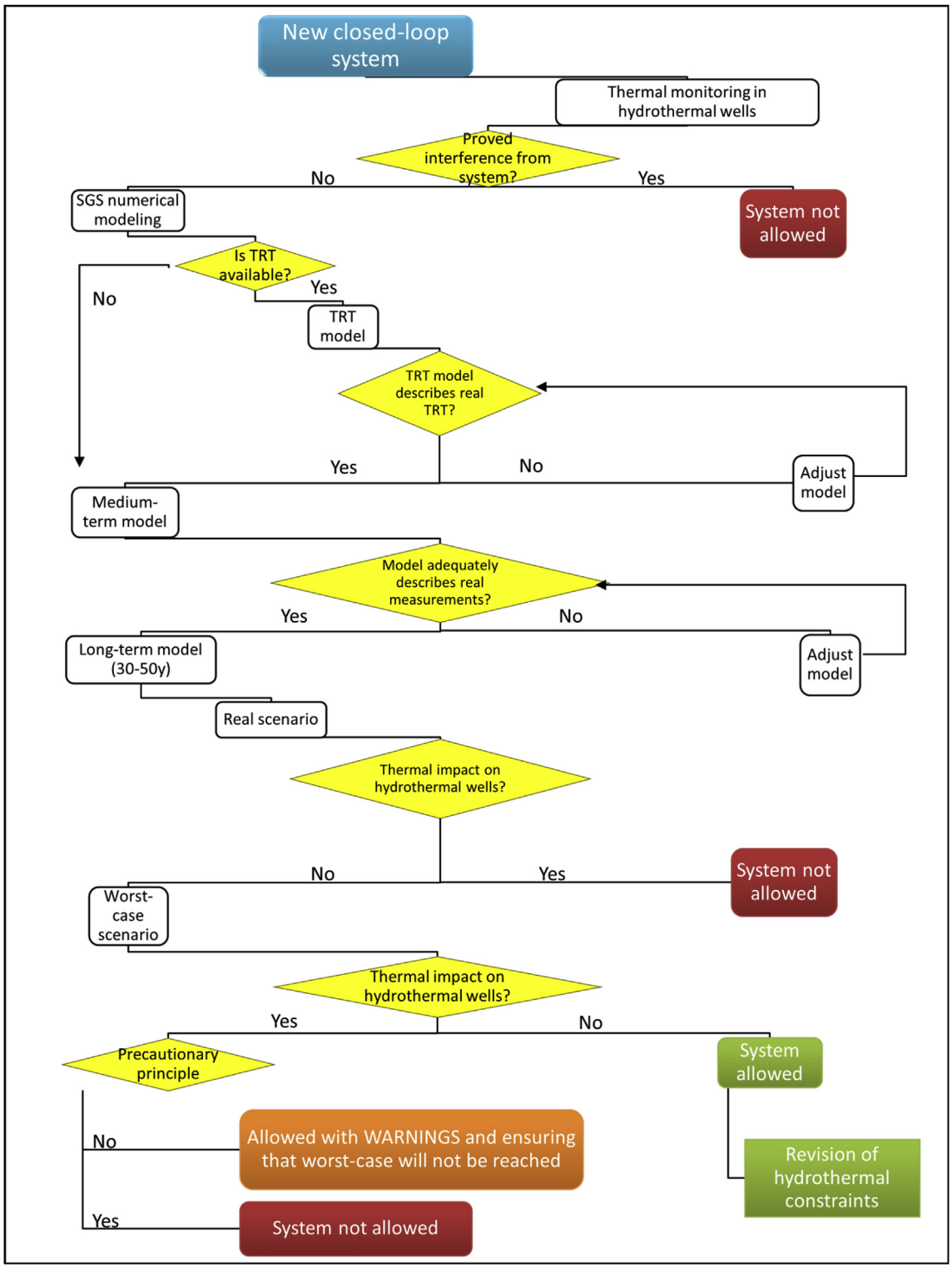

Fig. 5. Proposed framework to assess thermal sustainability of new closed-loop systems through monitoring and modeling in areas characterized by the presence of geothermal constraints.

dimensional mesh, obtaining a vertically extruded numerical model with an overall depth of 200m. The model was finally represented by almost 2,250,000 nodes and over 480,000 triangular prisms, with 4716 nodes per slice and 9295 elements per layer. This allowed obtaining a far field both horizontally (average distance between probes and borders of 50 m) and vertically (distance of 75 m from the probe feet to the lower limit of the model). The superficial 2D mesh and the full 3D model are reported in Fig. 6.

3.4.2. Material properties

As previously stated in paragraph 2.3 and in Ref. [20], the geological conceptual model can be schematized as composed of a

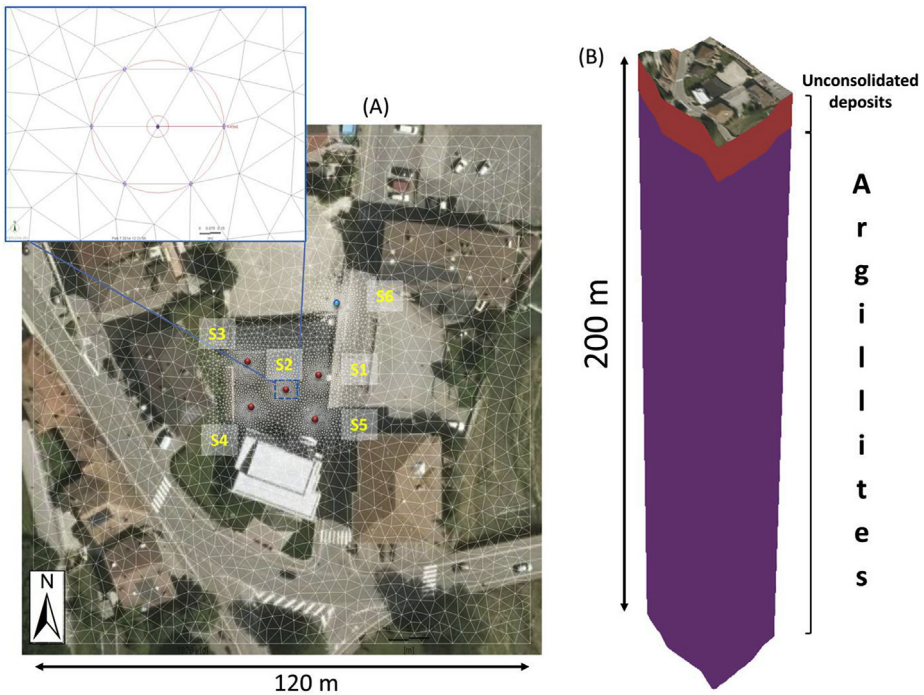

Fig. 6. A) 2D mesh, refined around the BHE array and optimized around each BHE. The BHE array is also highlighted: the active probes are reported in red while the monitoring site S6 is reported in light blue; B) 3D model with the different lithologies highlighted. (For interpretation of the references to colour in this figure legend, the reader is referred to the Web version of this article.)

layer of fluvio-glacial deposits with a thickness of approximately 10 m which covers a thick argillite formation. Hydrogeological and thermo-geological properties of the numerical model were derived from local studies, thematic bibliography and TRT data. Table 2 -reports the overall hydrogeological and thermo-geological properties that were used for all numerical simulations with the corresponding reference sources. It was chosen to simulate the whole domain as saturated, since vadose zone is negligible if compared to the rest of domain (less than 1.5% of the total domain depth). Such generalization supports a greater numerical stability. Longitudinal and transversal thermal dispersivities were respectively set to 5 m and 0.5 m (default values of FEFLOW) since no in-situ measurements were available to justify an adjustment of these values: however the value of thermal dispersivity varies depending on the scale of the analyzed phenomenon.

3.4.3. *Initial and boundary conditions*

Groundwater level has been obtained according to direct drilling investigation on site (S1), which stated that it is found at approximately 3 m below ground level. The groundwater hydraulic gradient was estimated according to the local hydrogeological condition and the available information (0.002) [41]. Moreover, it is assumed that the Sarca River drives the groundwater field, therefore the flow direction should locally stand South to North. A daily average heat-transfer boundary condition was set to the uppermost slice of the model, calculated from the values of hourly air temperature measured by the CEIS monitoring system. The geothermal flux was set on the lowest slice of the model (200m depth) as a heat flux boundary condition, simulating the rise of thermal energy from the Earth's interior with a magnitude of 0.05 W/m^2, considered as a representative value for the investigated local-scale area according to the heat flux map of Italy [42]. The initial temperature distribution was set based on the undisturbed temperature profile measured before the installation of the BHE array within the continuous core drilling S1 performed in 2013 [20], reported in Fig. 4 (A). The temperature profile at depths below 98 m b g.l. (not available due to the collapse of S1) was obtained using a constant geothermal gradient of 2 °C/100m, which corresponds to a geothermal flux of 0.05 W/m^2 when the average thermal conductivity of the underground is set at 2.5 W/mK. The BHEs were set between 0 and 125 m b.g.l. The heat exchangers were represented by double-U probes, installed in boreholes with a diameter of 152 mm. The chosen thermo-vector fluid was a mixture of water and monopropylene glycol 25%. The overall information on the numerical parameters used to model the BHEs are reported in the Supplementary Material Table SM1 while the boundary conditions used in the model are reported in Fig. 7.

4. Results

In the following, the results of the numerical modeling are divided into three steps: short-term response (the 70 h TRT model),

Table 2
Hydrogeological and thermogeological properties assigned to the numerical model.

Lithology	Longitudinal hydr. conductivity (m/s)	Transversal hydr. conductivity (m/s)	Ss (1/m)	ϕ	Λ (W/mK)	VHC (MJ/m^{3}K)	Long. th. dispersivity(1/m)	Transv. thermal disp.(1/m)
Fluvio-glacial deposits wet	0.00007	0.000007	1.65E^{-4} (dense sand)	0.26	2.69	2.23	5	0.5
Argillite	9E^{-10}	9E^{-11}	3.3E^{-6}	0.12	2.69	2.23	5	0.5
Source	[38]		[39]	[40]	TRT [29]		FEFLOW default	

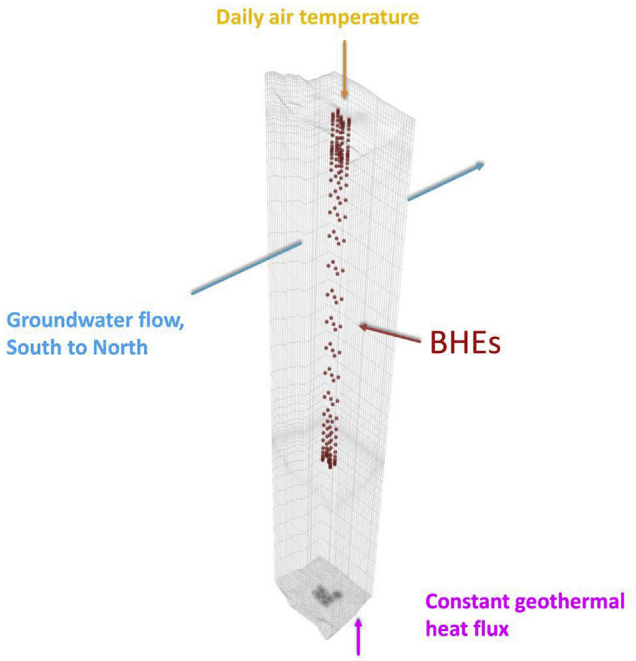

Fig. 7. Flow and heat transport boundary conditions applied to the numerical model.

medium-term impact (3 years simulation vs real operation), long-term impact (50 years simulation for real-case and heating-only scenario).

4.1. Short-term response: the TRT model

Firstly, the model was tested in order to understand its reliability in short-term response. The short-term analysis reproduced the exact conditions observed during the TRT performed on February 5th, 2014 (70 h). Therefore, the TRT scenario considered as active only the BHE S2, where the TRT test was executed. The initial temperature profile was derived from a steady-state simulation where air temperature was set to 4.6 °C (measured air temperature value at the beginning of the TRT), while to the deeper portion a constant temperature value of 13.5 °C was assigned, equal to the average undisturbed underground temperature measured by the TRT. Underground thermal properties were set accordingly to the measured values (thermal conductivity of 2.69 W/mK and volumetric heat capacity of 2.23 MJ/m^{3}K). It was chosen to specifically assign the measured borehole resistance to the BHE model (R_b = 0.1 mK/W), while the internal resistance R_a was assigned according to an EED analysis outcome [43] (0.4 mK/W). Air temperature, flow rate inside the BHE and inlet temperature were set as boundary conditions for the simulation according to real time measurements performed every 15 min during the TRT. Numerical solution of Al Khoury (2006) [37] was used to simulate a short-term and highly transient process as the TRT. Measured and computed outlet temperatures were used to assess the TRT model. The comparison is reported in Fig. 8: there is a small discrepancy during the first 12 h, quantified in maximum 0.7 °C. The MAE (Mean Absolute Error) and the RMSE (Root Mean Squared Error) between measured and simulated outlet temperatures were respectively of 0.5 and 0.8 °C. As a result, we can state that the model correctly supports a short-term TRT analysis.

4.2. Medium-term impact: 3 years simulation vs real operation

In the second phase of the current study, the numerical model was run for three years, from April 2nd, 2015 to March 31st, 2018, for a total of 1095 days, accordingly with the monitoring dataset. In the model, seven observation points were located in the passive BHE S6 (24 m North-East away from the BHE array barycenter), reproducing the temperature sensors which were placed in S6 with 20 m leg step, starting from the ground surface and down to a depth of 140 m. According to the monitoring dataset, the 10 min values of net power to the underground (heat extracted + heat injected, negative the first, positive the second) and thermo-vector fluid flow rate circulating in the probes were averaged over each day; these data were then used as input boundary conditions for the active BHE field (Fig. 9).

A sensitivity analysis focused on the evaluation of the thermal plume extent depending on the variation of some selected model parameters was performed. Hydraulic conductivity was increased by +25% and 50% compared to the initial one, thermal conductivity was increased by 10 and 25% compared to the initial one, volumetric heat capacity was increased of 10 and 20% and thermal dispersivity was set to 2.5m and 10m, respectively −50% and +50% than the initial one. The extent of the thermal perturbation was assessed within the argillites at a depth of 76m, by measuring the extent of the produced thermal plume passing from the barycenter (S2). Isolines for 10.5 and 11 °C were considered in order to spatially assess the extent variation of the thermal plumes.

Results of the sensitivity analysis are reported as graphs in Fig. 10 and as maps in Supplementary Material (Figures SM 1, 2, 3 and 4). In Fig. 10 the x axis represent the % variation of the investigated parameter compared to the initial one and the y axis represent the variation on the thermal plume extent calculated as a percentage. As expected, increasing both longitudinal and transversal hydraulic conductivity by 25 and 50% (figure A) does not lead to a significantly increased size of the thermal plume (0.3–0.5%), since the geological framework is almost completely composed of argillites, which possess very low hydraulic conductivity. Increasing thermal conductivity of the solid matrix by 10 and 20% (figure B) increases the heat exchange between the BHEs and the surrounding ground, producing a minor thermal alteration and a smaller thermal plume, as also explained in Ref. [44]. In this case increasing thermal conductivity by 10 and 20% (from 2.69 of the default to 2.96 and 3.2 W/mK) produced a reduction of the thermal plume respectively by 2 and 5.6%. The increase of volumetric heat capacity by 10 and 20% (figure C, from 2.23 of the default to 2.5 and 2.7 MJ/m^{3}K) does not substantially affect the extent of the thermal plume, with negligible decrease between 0.8 and 1%. The increase of both longitudinal and transversal thermal dispersivities within a reasonable range of 2.5–10 m, commonly used in literature [44,45] (figure D) seems to produce a slightly larger thermal plume, but the variation is comprised within 2% of the initial extent. Thermal dispersivity is a difficult parameter to estimate for real-scale BHEs and it also depends on the scale of the investigated phenomenon, therefore its setting is always problematic. In this case the increase or decrease of the thermal dispersivity by 50% does not substantially affects the extent of the thermal plume, stating that it is not a critical parameter for the analyzed case study.

It follows from the sensitivity analysis that the main parameter affecting the extent of the thermal plume for an almost purely conductive phenomenon such as the simulated one (due to the negligible presence of saturated fluvio-glacial sediments where advection takes place, compared to the extent of the sedimentary bedrock with argillites) is the thermal conductivity of the medium, that was previously experimentally assessed with a TRT.

After the execution of the sensitivity analysis, the model reliability was therefore assessed by comparing measured and simulated data: GSHP inlet/outlet temperatures in time, underground temperature detected in time at the seven observation points along

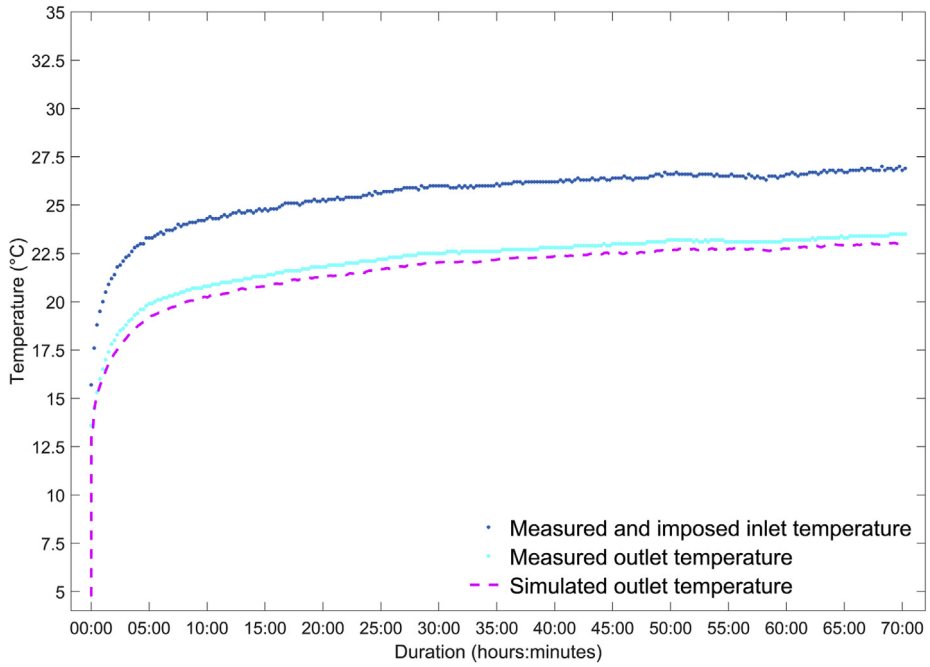

Fig. 8. Comparison between measured and simulated outlet temperatures for the TRT model.

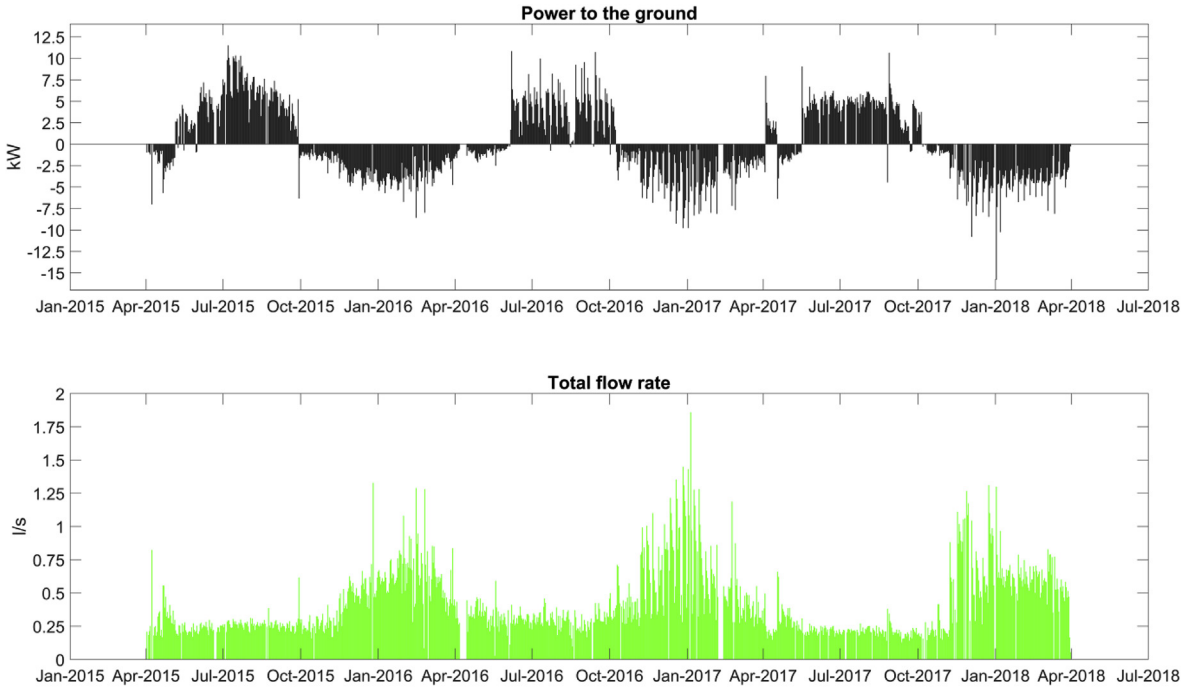

Fig. 9. Daily averaged boundary conditions assigned to the BHE field within the 3 years numerical model: top) power to the underground (positive = cooling demand; negative = heating demand); bottom) total flow rate circulating in the 5 probes.

S6 and thermal profiles at different times. Results of the inlet and outlet temperatures of the three-years model are reported in Fig. 11. Measured inlet and outlet temperatures are reported as hourly data, while modelled ones are reported as daily results. Results show that the simulated inlet temperatures are very close to the measured ones, while the simulated outlet temperatures are often slightly lower than the measured ones, particularly for the summer period.

The second comparison was performed by assessing the discrepancy between measured and simulated underground temperatures in probe S6 at different depths and considering the three-year simulation period. The analysis is reported in Fig. 12.

Overall accuracy between measured and modelled temperature at each depth is good, since the discrepancy is generally comprised within ±0.5 °C and often comprised within the temperature measurement error (±0.21 °C). A similar comparison was performed

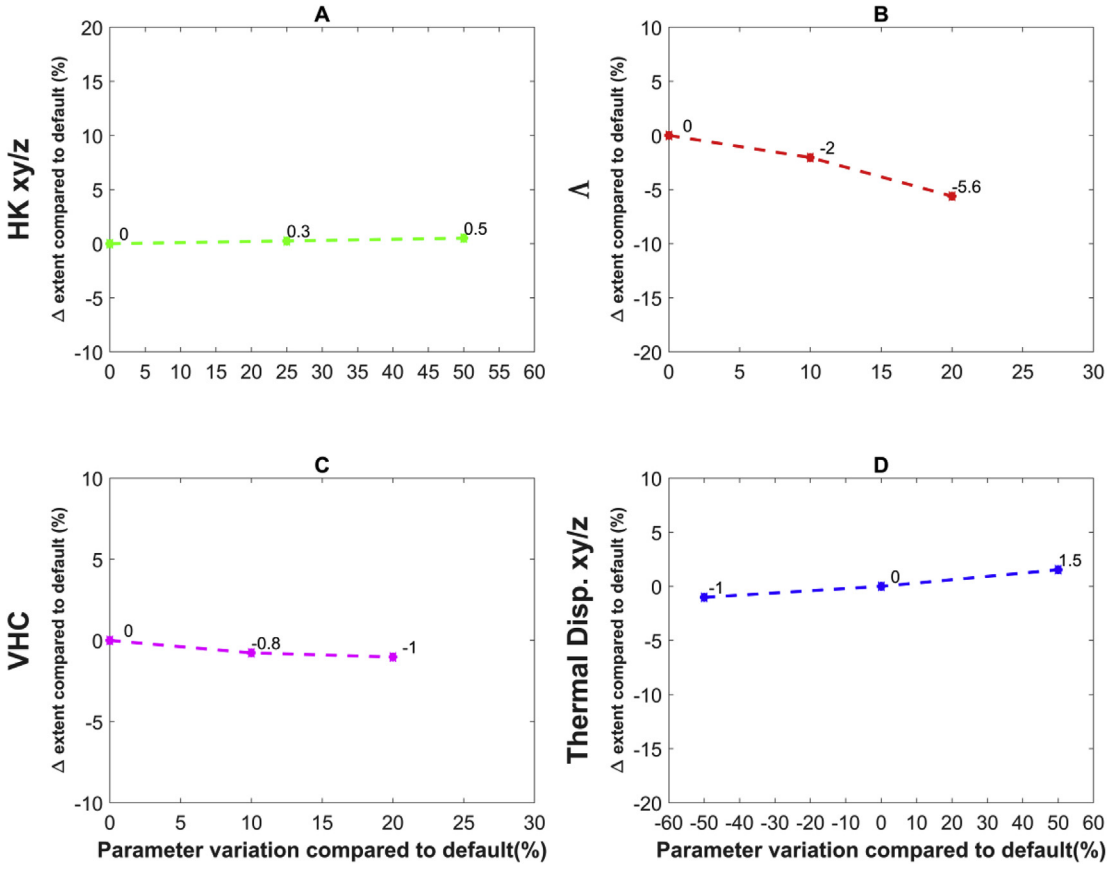

Fig. 10. Sensitivity analysis for some of the numerical 3 years model parameters: A) longitudinal and transverse hydraulic conductivity; B) thermal conductivity; C) volumetric heat capacity; D) longitudinal and transverse thermal dispersivity. The analysis was performed by evaluating the extent of a certain temperature isoline varying different parameters.

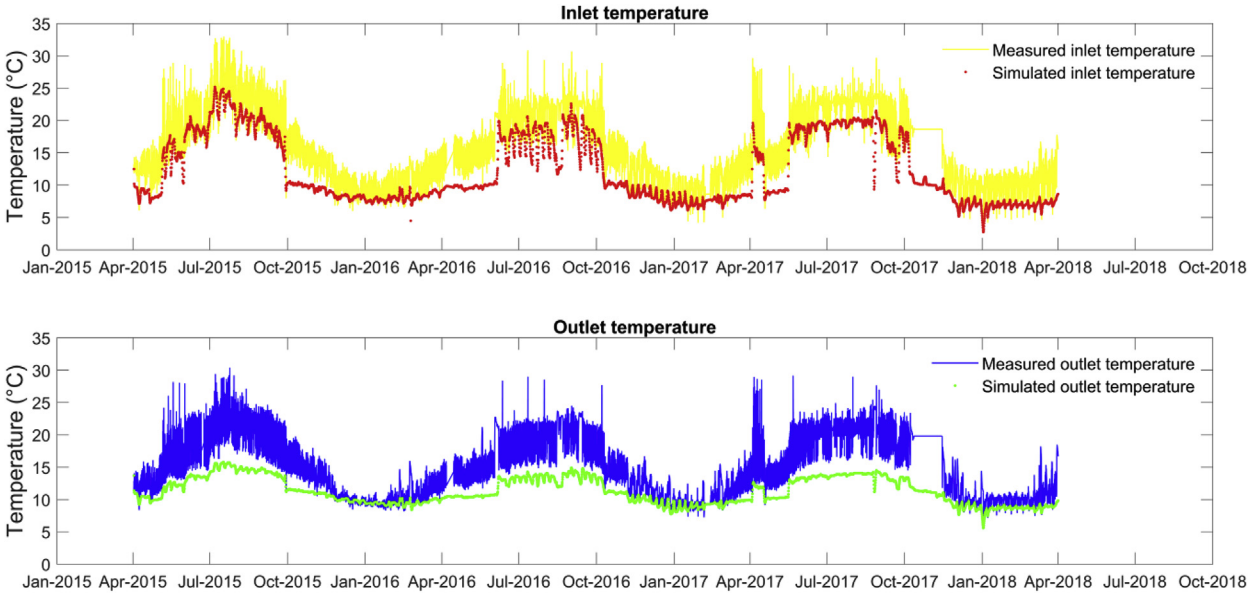

Fig. 11. Comparison between hourly measured inlet and outlet temperatures (respectively in yellow and blue) against simulated daily inlet and outlet temperatures (respectively in red and green) during 3 years of monitoring. (For interpretation of the references to colour in this figure legend, the reader is referred to the Web version of this article.)

using S6 measured and simulated temperature profiles in six different times: end of 2015, July 2016, end of 2016, July 2017, end of 2017 and end of the simulation (end of March 2018) (see also the scatter plot reported in Supplementary Material, Figure SM5). This was chosen to understand the vertical behavior of the model during winter heating and summer cooling periods. The comparison, reported in Fig. 13, shows a reliable representation of the real operation by the FEFLOW model: simulated thermal profiles are in good agreement with the measured ones with both MAE and RMSE being 0.4-0.5 °C at most.

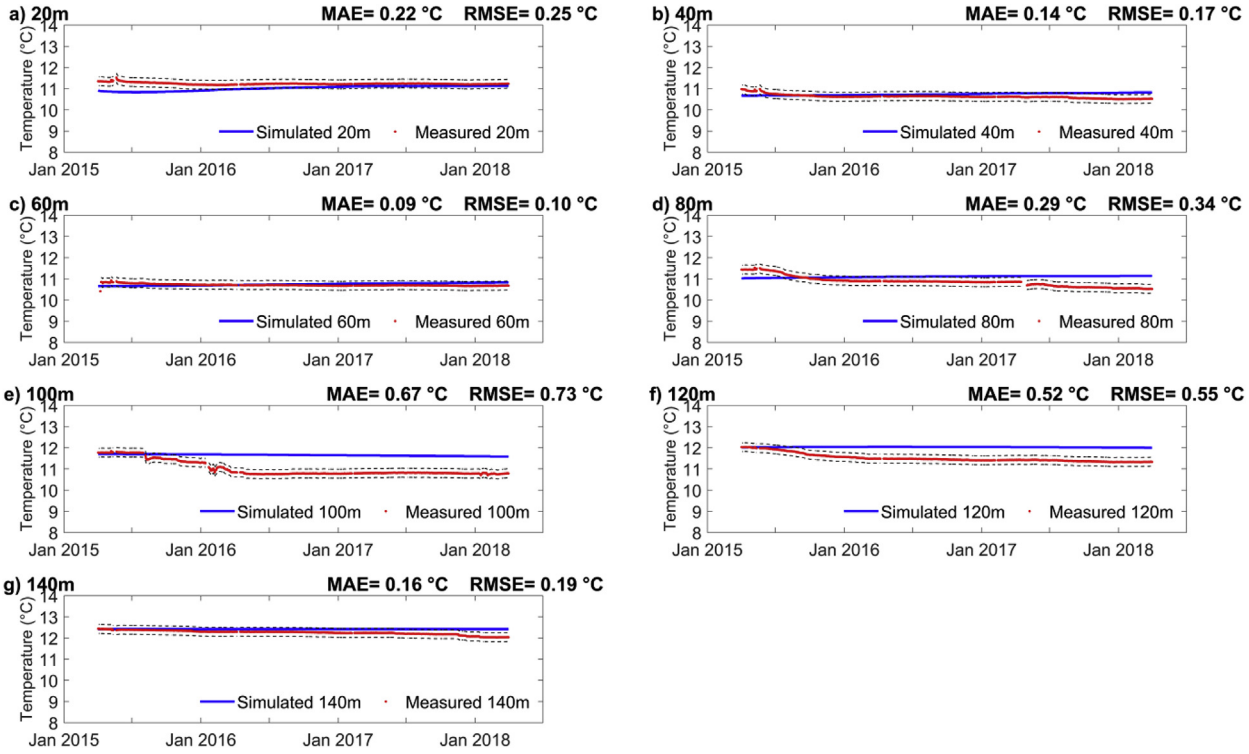

Fig. 12. Comparison between measured (red) and simulated (blue) daily underground temperatures during 3 years. The observation points were located in the S6 probe at different depths. The black dashed lines represent the total error of the temperature sensors (±0.21 °C). For each depth, the Mean Absolut Error (MAE) and the Root Mean Squared Error (RMSE) are reported. (For interpretation of the references to colour in this figure legend, the reader is referred to the Web version of this article.)

Fig. 14 represents the extent of the thermal plumes at depth of 76m developed by the geothermal system operation after the 3rd cooling period (October 1st, 2017, figure A) and after the 3rd heating period (which is also the end of the 3 years simulation, April 1st, 2018, figure B). The extent of the plume is the maximum extension of the thermal alteration compared to initial conditions. It can be seen that the extent the two plumes is very limited, in particular the hot plume produced from summer season cooling is limited to a diameter of 28 m from the barycenter (probe S2) while the cold plume produced by winter season heating is limited to a diameter of 39 m. The real temperature measurements coming from the S6 monitoring system highlight the absence of thermal perturbation produced by the geothermal system. This is also well-caught by the numerical model.

In light of the multiple verifications and performed analysis for both short-term and medium-term scenarios, the produced flow and transport model was considered as reliable and suitable for further long-term forecast simulations.

4.3. Long-term impact: 50 years simulation for the real-case scenario

Long-term scenarios were performed simulating for 50 years the behavior of the geothermal bore field, both in real energy demand conditions (balanced) and in a heating only scenario (strongly unbalanced), to understand the potential thermal issues caused by the system towards hydrothermal protection areas at real and heating-only conditions. From the three-years monitoring dataset, the 10-min values of net power and thermo-vector fluid flow rate were averaged monthly and repeated cyclically during 50 years, representing boundary conditions for the BHE field. Fig. 15 reports the results of the 50-years simulation with real, balanced energy demand, in terms of inlet/outlet temperatures and underground ones in S6 for different depths. It can be noted that the simulated inlet and outlet temperatures of the probe field do not show any clear long-term thermal drift. Observation points set in the numerical model show that the temperature tends to remain stable, which is in agreement with the monitored thermal power to the ground, almost completely balanced during 3-years monitoring. The small simulated oscillations are produced by the cyclic arrival of a slightly hot or cold thermal plume produced by the geothermal system at S6. To assess the underground thermal alteration, the undisturbed temperature monitored in S6 at 80 m was considered as a referential starting point. By using this approach the maximum thermal alteration produced by the probe field in 50 years was quantified in +0.3 °C, showing that the system would basically produce a slight net injection of heat in the underground during this period. Fig. 16 reports the entity and shape of the simulated thermal plume after 50 years at 76 m depth, which is limited to an extent of approximately 74 m, calculated passing from the barycenter of the bore field (probe S2, as shown in Fig. 2). In particular, Fig. 16 compares the simulated thermal plume with the geothermal constraints map for Ponte Arche. From the outcomes of the 50 years simulation, it can be seen that the installed BHE field would not affect the existing hydrothermal wells at all. This can be mainly explained by the considerable distance of the hydrothermal wells from the geothermal system: Pozzo Dinosauro is in fact 610 m distant from the bore field, while Hydra1 and Antica Fonte are respectively 1350 and 1450 m away from the geothermal system.

4.4. Long-term impact: 50 years simulation for the heating-only scenario

Fig. 17 reports the results of the 50-years simulation in a virtual “worst case” heating-only scenario. Basically, this simulation only considers the heating load of the previous 50-years real case simulation, excluding the cooling load. In this case inlet and outlet temperatures show a visible thermal drift during the first 5 years of

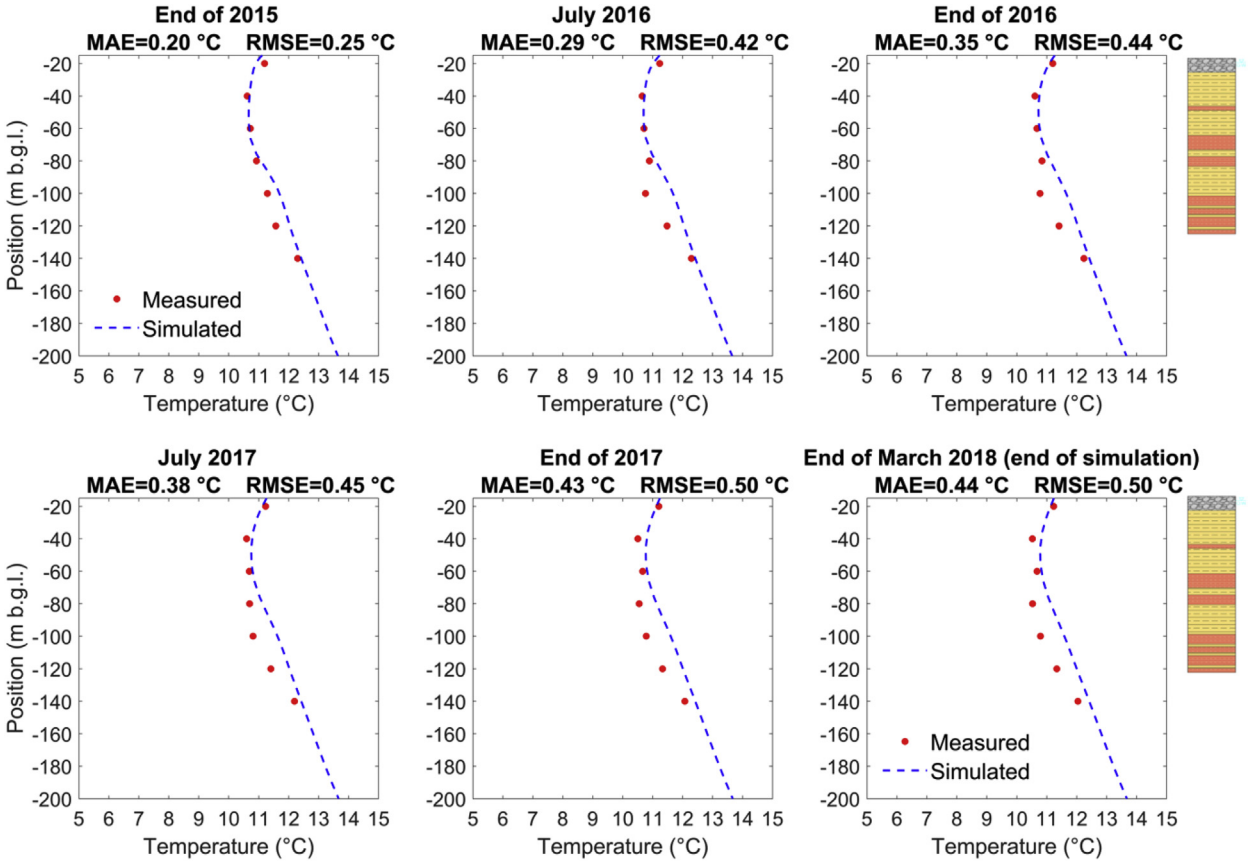

Fig. 13. Comparison between measured and simulated thermal profiles in six different times at probe S6 (3 years model); local stratigraphy in S1 is reported near the graphs. Fluvio-glacial deposits are represented in grey, compact marly clays in yellow and fractured marly clays in orange. (For interpretation of the references to colour in this figure legend, the reader is referred to the Web version of this article.)

Fig. 14. Thermal plumes at 76m depth developed after the 3rd cooling period (October 1st, 2017, figure A) and after the 3rd heating period (April 1st, 2018, figure B). The violet star represents the location of the observation points (probe S6). The transparent dashed white line represents the measurement of the thermal plume extension. (For interpretation of the references to colour in this figure legend, the reader is referred to the Web version of this article.)

simulation, where a slight decrease in temperature is observed. After five years the trend tends to stabilize, testifying that the geothermal system has reached a thermal equilibrium with the surrounding underground, also proving that the thermal properties of the subsurface can stand 50 years operation of the BHEs system even for an imbalanced thermal load. Considering a depth of 80 m the initial undisturbed underground temperature in S6 at the beginning of the simulation is 11 °C: after 50 years, in the heating-only scenario, the same monitoring point reaches a temperature of approximately 9.7 °C, with a temperature decrease of −1.3 °C. Fig. 18 shows the overall influence of the thermal plume, which is limited to an extent of 96 m, this means that even in this worst case scenario the thermal impact will not realistically reach the hydro-thermal wells.

5. Discussion

The 3D groundwater flow and heat transport model, built using the commercial software FEFLOW, combined short-term (70 h), medium-term (3 years) and long-term (50 years) analysis to demonstrate the overall thermal sustainability of the installed BHE system, assessing that no potential harm could be caused towards the hydrothermal wells. The TRT was adequately reproduced by the numerical model, obtaining MAE and RMSE of respectively 0.5 and

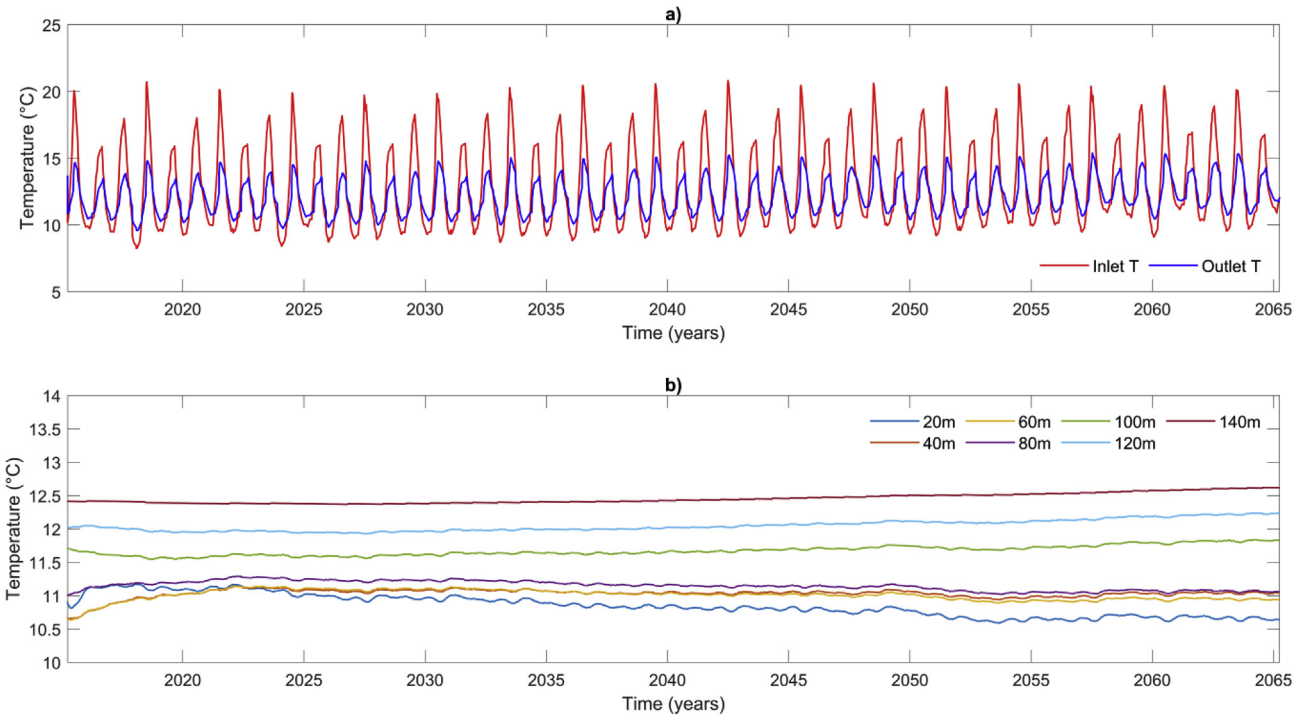

Fig. 15. The upper figure (a) reports probe inlet and outlet temperatures (respectively in red and blue) for the 50 years simulation using real case energy demand, while the lower figure (b) reports the underground temperatures simulated in S6 for seven different depths. (For interpretation of the references to colour in this figure legend, the reader is referred to the Web version of this article.)

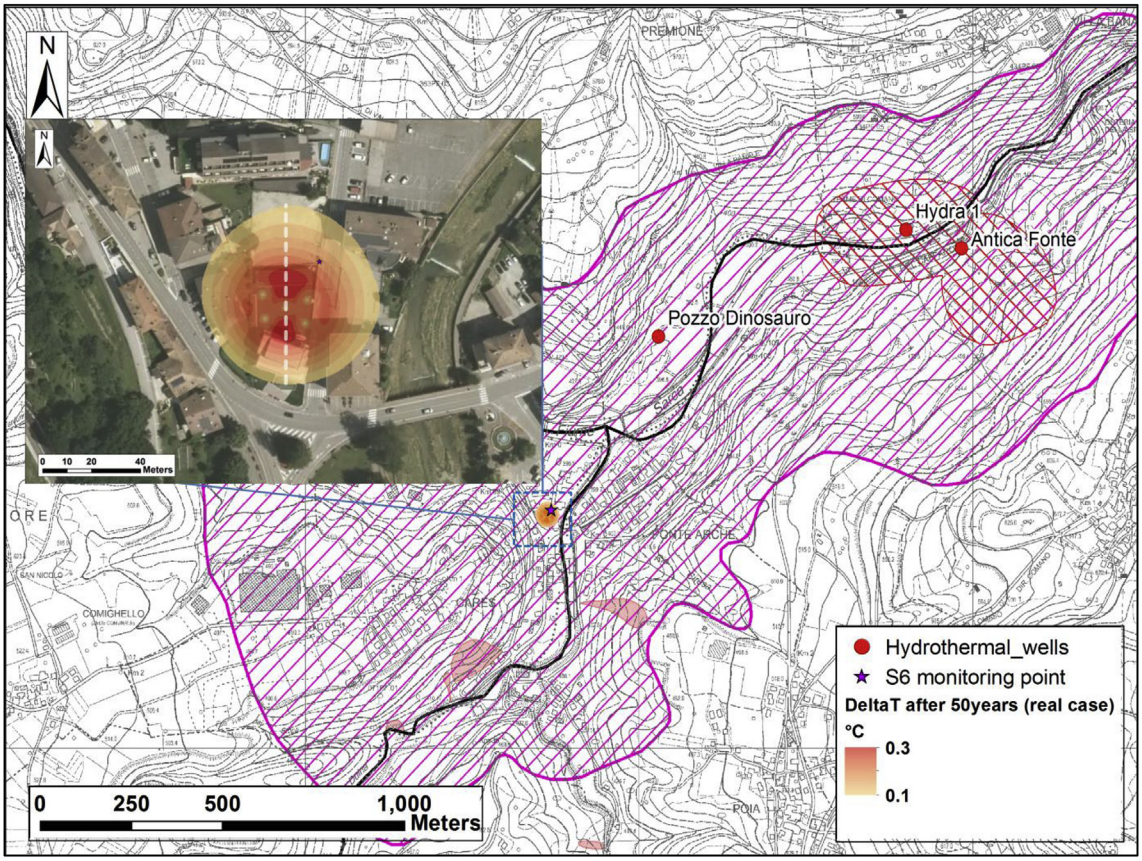

Fig. 16. Comparison of the extension of the modelled thermal plume, expressed as variation after 50 years of simulation from the initial temperature at z = −76m, with the location of the hydrothermal wells Pozzo Dinosauro, Hydra 1 and Antica Fonte. No influence of the BHE system towards these hydrothermal wells should be observed.

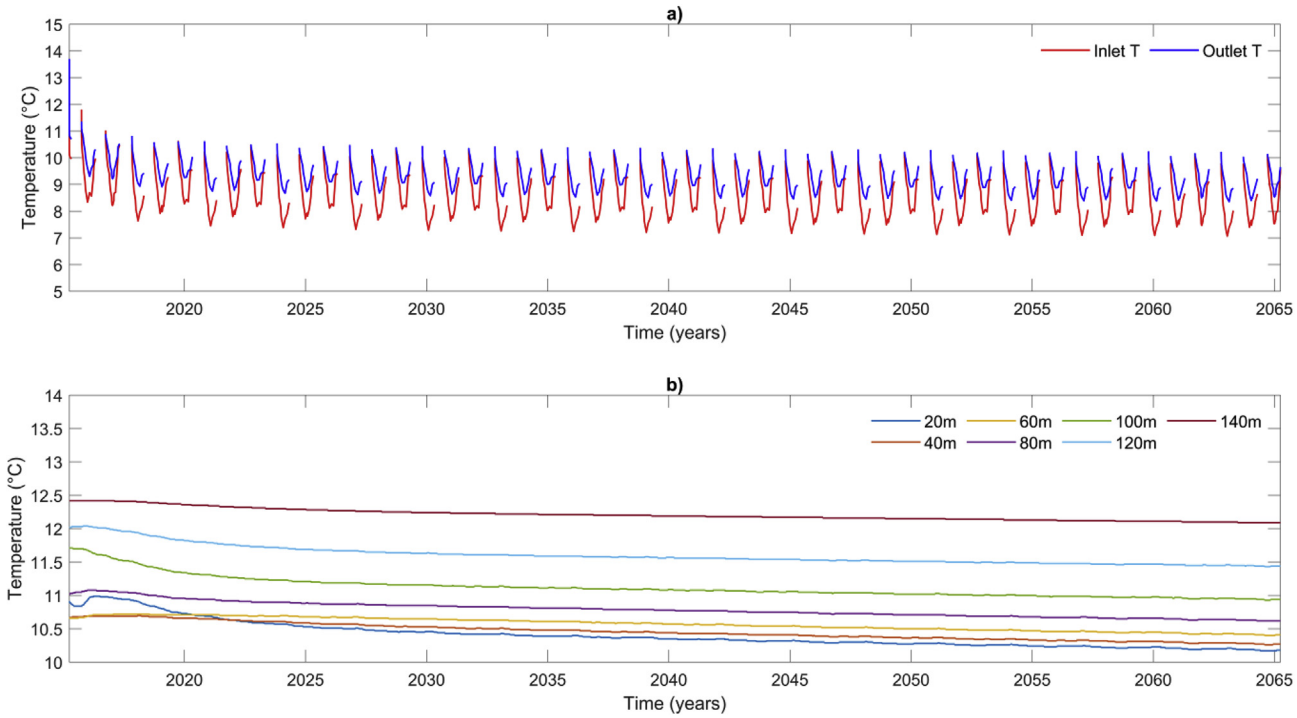

Fig. 17. The upper figure (a) reports inlet and outlet temperatures (respectively in red and blue) for the 50 years simulation with heating demand only, while the lower figure (b) reports the underground temperatures simulated in S6 at seven different depths for this scenario. Time periods in figure a) that do not show the presence of both inlet and outlet temperatures correspond to periods where the system is turned off, because no cooling is foreseen. (For interpretation of the references to colour in this figure legend, the reader is referred to the Web version of this article.)

0.8 °C between measured and simulated outlet temperatures, proving that it could well describe short-term geo-exchange phenomena. The TRT model was also used to understand if proper mesh quality was achieved, since the reproduction of such short-term test is numerically challenging and an accurate mesh design and optimization is required.

The assessment of the model reliability for a medium-term heat exchange process was subsequently performed by comparing simulated inlet/outlet and underground temperatures against measured ones. The shift between three-years measured and simulated inlet/outlet temperatures can first of all be ascribed to the fact that, to stay in reasonable computational times (approximately 9 h of computing time for the three-years simulation) and to reach numerical stability, power and flow rate were set as daily average boundary conditions instead of hourly values, losing peak values and part of the highly transient behavior. Moreover, the model seems to better describe the thermal behavior in winter, where both inlet and outlet simulated temperatures are in strong agreement with the measured ones. Instead, in summer, while the simulated inlet temperature is very close to the measured one the simulated outlet is lower than the measured one, suggesting a better geo-exchange performance of the simulated system than the real one especially in summer, since higher heat exchange with the underground produces a greater difference between inlet and outlet temperatures. However, despite these limitations, the three-year simulated inlet/outlet temperature trends are in satisfactory agreement with the measured ones, proving that the proposed model appropriately reproduces the ground side behavior of the system in a medium-term period.

The performed sensitivity analysis stated that large variations of hydraulic conductivity, volumetric heat capacity and thermal dispersivity do not substantially affect the extent of the thermal plume, while small variations of +10 and + 20% in thermal conductivity led to a decrease of its extent of 2 and 5.6%. The thermal conductivity values of the numerical model was however assigned based on a performed TRT, which returned a thermal conductivity of 2.69 W/mK and a R_b of 0.1 mK/W.

The reproduction of the measured temperatures at various depths by the 3 years numerical model is equally good. Average MAE and RMSE both lie around 0.4 °C, which can be considered as a good overall result, considered the complex lithological and hydrogeological framework, which is presumably characterized by groundwater flow in fractures and by the partial influence of neighboring surface water bodies.

The discrepancies observed at 100 and 120 m depth can be due to the movement of slightly colder groundwater arriving from nearby, particularly where the fracturation of the argillites creates some preferential pathways where it can flows at higher velocities: this is not well caught by the numerical model also because the local hydrogeological framework and the local interactions between surface water and groundwater were little known. The hypothesis is that there are some local heterogeneities in the lithology, mainly vertically, which cause underground temperature variations. The flow in fractured rocks could also be studied in order to more accurately characterize the hydrogeological behavior. The geological setting is almost completely characterized by the presence of sedimentary rocks, therefore the flow in saturated porous media should not be determinant for the characterization of the thermal plume. Moreover the small thermal plume produced in the unconsolidated layer would be engulfed by the two nearby surface water bodies, the Duina and Sarca rivers, which will act as hydraulic barriers.

The 50 years numerical simulation with the real case balanced energy demand leads to a slight net heat injection in the ground, resulting in a slight positive thermal drift. The simulation shows that the thermal plume developed after 50 years is limited to the proximity of the BHE field, approximately with a maximum extent of 74m calculated passing from the barycenter of the BHE field

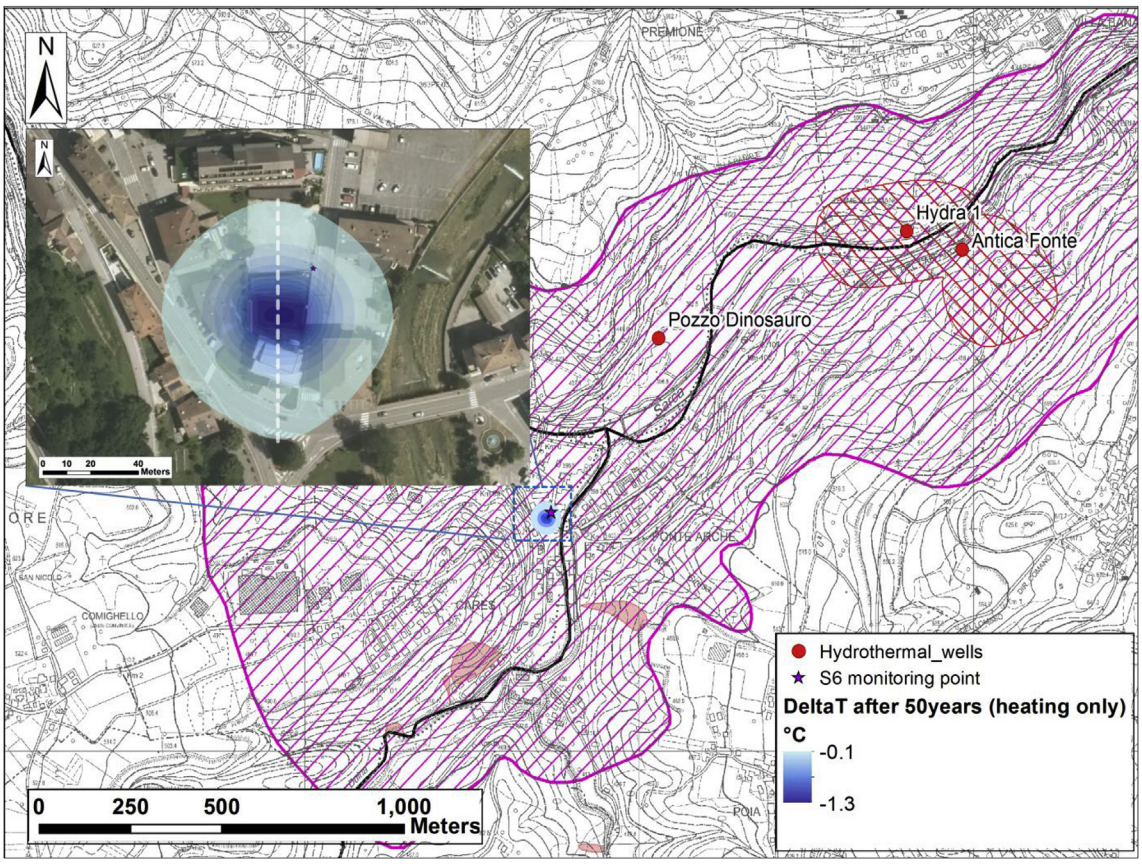

Fig. 18. Comparison of the extent of the modelled thermal plume for the heating-only scenario, expressed as variation after 50 years of simulation from the initial temperature at $z = -76$m, with the location of the hydrothermal wells Pozzo Dinosauro, Hydra 1 and Antica Fonte. No influence of the BHE field in these wells should be observed even in the worst-case scenario.

(probe S2). The low (and balanced) energy demand, the limited thickness of the fluvio-glacial cover and therefore the overall limited groundwater flow velocity do not support a thermal plume expansion in the long-term. Even considering the hypothesis of a long-term strongly imbalanced heating-only scenario, which theoretically represents a worst case, there would not be any critical consequence towards the hydrothermal wells because the thermal plume is limited to a maximum extent of 96 m of diameter.

6. Conclusions

Based on a real case study (Ponte Arche, Italy), this paper tests a procedure to assess if a pilot closed-loop shallow geothermal system could be considered as sustainable in the presence of hydrothermal constraints, namely if it would not produce thermal interference. The work also presents and discusses the coupling of high-resolution geothermal monitoring results and 3D numerical modeling to evaluate the potential influence of a BHE field on neighboring thermal baths, which are 610, 1350 and 1450 m distant.

The TRT and the three-years thermal and energetic data were used to calibrate both hydrogeological and thermal parameters within the numerical model.

Sensitivity analysis showed that great variations of hydraulic conductivity, volumetric heat capacity and thermal dispersivity do not substantially affect the extent of the thermal plume. Thermal conductivity seems to be the major parameter to consider for this case study, and it was therefore empirically assessed through a TRT. The three-years system operation implemented in the model show that the thermal impact on the subsurface is limited, due to the low and balanced yearly energy demand of the CEIS building and due to the geological framework where the BHE field is installed, dominated by the presence of a sedimentary bedrock. The created numerical model adequately simulated the monitored inlet/outlet temperatures in the probes and even the monitored underground temperatures in S6, with average MAE and RMSE of 0.4-0.5 °C. The developed hot and cold thermal plumes after three complete cooling and heating cycles have a spatial extent of respectively 28 and 39m, considering the measurement as in Fig. 14.

The long-term (50 years) simulation for the real case shows that the system does not substantially affects the underground temperature even at small distances: the slightly hot thermal plume (+0.3 °C maximum) shows an extent of approximately 74m and has its center in probe S2. When analyzing the results of the 50 years heating-only scenario, the thermal drift simulated after 50 years is slightly negative and the maximum extent of the cold plume is 96m. From modeling results it is realistic to say that no long-term significant alteration is expected in the hydrothermal wells neither for both a real-case scenario nor for a hypothesis of a heating-only one. In light of these outcomes, a revision of the hydrothermal constraints is suggested to potentially install new systems. Based on both monitoring (CEIS building and hydrothermal wells[1]) and modeling results, the local geological survey is

[1] The hydrothermal wells monitoring data (not publishable) shows no changes that could be correlated to the operation of the CEIS geothermal plant; this justifies the authorization to CEIS to continue the experimentation.

considering how to adapt the authorization regulations, allowing the safe construction of further shallow geothermal systems in the hydrothermal protected area.

This proposed approach can be a guideline for the scientific community and for the public bodies in the evaluation and promotion of the shallow geothermal energy through closed-loop systems as a sustainable, efficient and renewable and energy source which could speed up the local energy transition from fossil fuels to renewable energy.

Declaration of competing interest

The authors declare that they have no known competing financial interests or personal relationships that could have appeared to influence the work reported in this paper.

CRediT authorship contribution statement

Rodolfo Perego: Writing - original draft, Conceptualization, Data curation, Formal analysis, Investigation. **Diego Viesi:** Investigation. **Sebastian Pera:** Project administration, Funding acquisition. **Giorgia Dalla Santa:** Writing - review & editing. **Matteo Cultrera:** Conceptualization, Supervision. **Paola Visintainer:** Project administration. **Antonio Galgaro:** Funding acquisition, Supervision.

Acknowledgments

The authors would like to thank the Geological Survey of the Autonomous Province of Trento and CEIS for providing the data required to build a complex numerical model. The authors would like to thank the anonymous reviewers for their constructive and positive reviews, which certainly helped in greatly improving the paper.

Appendix A. Supplementary data

Supplementary data to this article can be found online at https://doi.org/10.1016/j.renene.2020.02.068.

References

[1] D. Banks, An Introduction to Thermogeology: Ground Source Heating and Cooling, second ed., John Wiley & Sons, 2012 https://doi.org/10.1002/9781118447512.
[2] N. Goldscheider, T.D. Bechtel, Editors' message: the housing crisis from underground—damage to a historic town by geothermal drillings through anhydrite, Staufen, Germany, Hydrogeol. J. 17 (3) (2009) 491–493, https://doi.org/10.1007/s10040-009-0458-7.
[3] P. Blum, G. Campillo, T. Kölbel, Techno-economic and spatial analysis of vertical ground source heat pump systems in Germany, Energy 36 (2011) 2002–2011, https://doi.org/10.1016/j.energy.2011.02.044.
[4] S. Hähnlein, P. Bayer, G. Ferguson, P. Blum, Sustainability and policy for the thermal use of shallow geothermal energy, Energy Pol. 59 (2013) 914–925, https://doi.org/10.1016/j.enpol.2013.04.040.
[5] R. Perego, S. Pera, A. Galgaro, Techno-Economic mapping for the improvement of shallow geothermal management in southern Switzerland, Energies 12 (2019) 279.
[6] J.A. Rivera, P. Blum, P. Bayer, Analytical simulation of groundwater flow and land surface effects on thermal plumes of borehole heat exchangers, Appl. Energy 146 (2015) 421–433, https://doi.org/10.1016/j.apenergy.2015.02.035.
[7] H. Fujii, T. Inatomi, R. Itoi, Y. Uchida, Development of suitability maps for ground-coupled heat pump systems using groundwater and heat transport models, Geothermics 36 (5) (2007) 459–472, https://doi.org/10.1016/j.geothermics.2007.06.002.
[8] P. Hein, O. Kolditz, U.J. Görke, A. Bucher, H. Shao, A numerical study on the sustainability and efficiency of borehole heat exchanger coupled ground source heat pump systems, Appl. Therm. Eng. 100 (2016) 421–433, https://doi.org/10.1016/j.applthermaleng.2016.02.039.
[9] F. Tang, H. Nowamooz, Long-term performance of a shallow borehole heat exchanger installed in a geothermal field of Alsace region, Renew. Energy 128 (A) (2018) 210–222, https://doi.org/10.1016/j.renene.2018.05.073.
[10] N. Daemi, M.M. Krol, Impact of building thermal load on the developed thermal plumes of a multi-borehole GSHP system in different canadian climates, Renew. Energy 134 (2019) 550–557, https://doi.org/10.1016/j.renene.2018.11.074.
[11] G. Dalla Santa, Z. Farina, H. Anbergen, W. Rühaak, A. Galgaro, Relevance of computing freeze-thaw effects for borehole heat exchanger modelling: a comparative case study, Geothermics 79 (2019) 164–175, https://doi.org/10.1016/j.geothermics.2019.02.001.
[12] J. Epting, F. Händel, P. Huggenberger, Thermal management of an unconsolidated shallow urban groundwater body, Hydrol. Earth Syst. Sci. 17 (2013) 1851–1869, https://doi.org/10.5194/hess-17-1851-2013.
[13] M. Cultrera, J. Boaga, E. Di Sipio, G. Dalla Santa, M. De Seta, A. Galgaro, Modelling an induced thermal plume with data from electrical resistivity tomography and distributed temperature sensing: a case study in northeast Italy, Hydrogeol. J. 26 (3) (2018) 837–851, https://doi.org/10.1007/s10040-017-1700-3.
[14] A. Galgaro, Z. Farina, G. Emmi, M. De Carli, Feasibility analysis of a Borehole Heat Exchanger (BHE) array to be installed in high geothermal flux area: the case of the Euganean Thermal Basin, Italy, Renew. Energ. 78 (2015) 93–104, https://doi.org/10.1016/j.renene.2014.11.076.
[15] M. Goodarzi, S.S. Eslamian, Evaluation of WhAEM and MODFLOW models to determine the protection zone of drinking wells, Environ. Earth Sci. 78 (2019) 195, https://doi.org/10.1007/s12665-019-8204-5.
[16] K.N. Moutsopoulos, A. Gemitzi, V.A. Tsihrintzis, Delineation of groundwater protection zones by the backward particle tracking method: Theoretical background and GIS-based stochastic analysis, Environ. Geol. 54 (5) (2008) 1081–1090, https://doi.org/10.1007/s00254-007-0879-3.
[17] N.N. Kourgialas, G.P. Karatzas, G.C. Koubouris, A GIS policy approach for assessing the effect of fertilizers on the quality of drinking and irrigation water and wellhead protection zones (Crete, Greece), J. Environ. Manag. 189 (2017) 150–159, https://doi.org/10.1016/j.jenvman.2016.12.038.
[18] Y. Liu, N. Weisbrod, A. Yakirevich, Comparative study of methods for delineating the wellhead protection area in an unconfined coastal aquifer, Water (Switzerland) 11 (6) (2019) 1168, https://doi.org/10.3390/w11061168.
[19] H.J.G. Diersch, FEFLOW: Finite Element Modeling of Flow, Mass and Heat Transport in Porous and Fractured Media, Springer Science & Business Media, 2013.
[20] D. Viesi, A. Galgaro, A. Zanetti, P. Visintainer, L. Crema, Experimental geothermal monitoring assessing the underground sustainability of GSHP borehole heat exchangers in a protected hydrothermal area: the case study of Ponte Arche (Italian Alps), Geothermics 75 (2018) 192–207, https://doi.org/10.1016/j.geothermics.2018.05.002.
[21] Sgi (Servizio Geologico d'Italia), Progetto CARG, Foglio 059 Tione di Trento, 2010.
[22] M. Nardin, L. Veronese, Il campo geotermico di Comano (fluidi a Bassa entalpia). Quindici anni di ricerche del Servizio Geologico della Provincia Autonoma di Trento, I Quaderni del Servizio Geologico della PAT, 1994.
[23] R. Perego, R. Guandalini, L. Fumagalli, F.S. Aghib, L. De Biase, T. Bonomi, Sustainability evaluation of a medium scale GSHP system in a layered alluvial setting using 3D modeling suite, Geothermics 59 (A) (2016) 14–26, https://doi.org/10.1016/j.geothermics.2015.10.003.
[24] PAT 2013 (Autonomous Province of Trento), Delibera n. 1593 del 2/8/2013. Approvazione del primo aggiornamento della 'Carta delle limitazioni per l'installazione di sonde geotermiche a circuito chiuso', 2013.
[25] http://www.termecomano.it/en, Last Access: 04/02/2020, [Online].
[26] Geological Service Trentino, Indagini geofisiche in foro per la progettazione dell'impianto geotermico a servizio della sede CEIS in via San Giovanni Bosco a Ponte Arche, 2013.
[27] Richtlinienreihe VDI 4640 Thermische Nutzung des Untergrunds, 2000.
[28] A. Capozza, M. De Carli, A. Galgaro, A. Zarrella, Linee Guida per la progettazione dei campi geotermici per pompe di calore, Rapporto RSE 12000317, 2011.
[29] F. Vendrame, Test di Risposta Termica su sonda geotermica in pozzo verticale, località Ponte Arche via S, Giovanni Bosco, 2014.
[30] C. Lee, M. Park, T.B. Nguyen, B. Sohn, J.M. Choi, H. Choi, Performance evaluation of closed-loop vertical ground heat exchangers by conducting in-situ thermal response tests, Renew. Energy 42 (2012) 77–83, https://doi.org/10.1016/j.renene.2011.09.013.
[31] N. Diao, Q. Li, Z. Fang, Heat transfer in ground heat exchangers with groundwater advection, Int. J. Therm. Sci. 43 (12) (2004) 1203–1211, https://doi.org/10.1016/j.ijthermalsci.2004.04.009.
[32] H. Wang, C. Qi, H. Du, J. Gu, Thermal performance of borehole heat exchanger under groundwater flow: a case study from Baoding, Energy Build. 41 (12) (2009) 1368–1373, https://doi.org/10.1016/j.enbuild.2009.08.001.
[33] G. Dalla Santa, A. Galgaro, R. Sassi, M. Cultrera, P. Scotton, J. Mueller, D. Bertermann, D. Mendrinos, R. Pasquali, R. Perego, S. Pera, E. Di Sipio, G. Cassiani, M. De Carli, A. Bernardi, An updated ground thermal properties database for GSHP application, Geothermics 85 (2018) 101758, https://doi.org/10.1016/j.geothermics.2019.101758.
[34] A.E. Dembe, C. Raffensperger, J. Tickner, Protecting public health and the environment: Implementing the precautionary principle, J. Publ. Health Pol. 22 (2) (2001) 236–238, https://doi.org/10.2307/3343463.
[35] H.J.G. Diersch, D. Bauer, W. Heidemann, W. Rühaak, P. Schätzl, Finite element formulation for borehole heat exchangers in modeling geothermal heating systems by FEFLOW, FEFLOW White Papers 5 (2010).

[36] P. Eskilson, J. Claesson, Simulation model for thermally interacting heat extraction boreholes, Numer. Heat Tran. 13 (2) (1988) 149–165, https://doi.org/10.1080/10407788808913609.
[37] R. Al-Khoury, P.G. Bonnier, Efficient finite element formulation for geothermal heating systems. Part II: Transient, Int. J. Numer. Methods Eng. 67 (2006) 725–745, https://doi.org/10.1002/nme.1662.
[38] P.A. Domenico, F.W. Schwartz, Physical and Chemical Hydrogeology, vol. 506, Wiley, New York, 1998.
[39] P.A. Domenico, M.D. Mifflin, Water from low-permeability sediments and land subsidence, Water Resour. Res. 1 (4) (1965) 563–576, https://doi.org/10.1029/WR001i004p00563.
[40] D.A. Morris, A.I. Johnson, Summary of hydrologic and physical properties of rock and soil materials, as analyzed by the hydrologic laboratory of the U.S, Geological Survey, 1967, pp. 1948–1960, https://doi.org/10.3133/wsp1839D.
[41] D. Viesi, A. Galgaro, P. Visintainer, L. Crema, GIS-supported evaluation and mapping of the geo-exchange potential for vertical closed-loop systems in an Alpine valley, the case study of Adige Valley (Italy), Geothermics 71 (2018) 70–87, https://doi.org/10.1016/j.geothermics.2017.08.008.
[42] Geothopica project - http://geothopica.igg.cnr.it.Last Access: 04/02/2020, [Online].
[43] G. Hellström, B. Sanner, Earth Energy Designer. User's Manual, Version, 2, 2000.
[44] A. Casasso, R. Sethi, Efficiency of closed loop geothermal heat pumps: a sensitivity analysis, Renew. Energy 62 (2014) 737–746, https://doi.org/10.1016/j.renene.2013.08.019.
[45] S. Lo Russo, G. Taddia, V. Verda, Development of the thermally affected zone (TAZ) around a groundwater heat pump (GWHP) system: a sensitivity analysis, Geothermics 43 (2012) 66–74, https://doi.org/10.1016/j.geothermics.2012.02.001.